



Characterization of trichome phenotypes to assess maturation and flower development in *Cannabis sativa* L. (cannabis) by automatic trichome gland analysis

D.B. Sutton ^{a,*}, Z.K. Punja ^b, G. Hamarneh ^a

^a School of Computing Science, Simon Fraser University, 8888 University Drive, Burnaby, B.C. V5A 1S6, Canada

^b School of Biological Sciences, Simon Fraser University, 8888 University Drive, Burnaby, B.C. V5A 1S6, Canada



ARTICLE INFO

Keywords:

Cannabis trichomes
Deep learning
Phenotype
Fluorescence
Precision agriculture

ABSTRACT

Cannabis (Cannabis sativa L.) is cultivated by licensed producers in Canada for medicinal and recreational uses. The recent legalization of this plant in 2018 has resulted in rapid expansion of the industry, with greenhouse production representing the most common method of cultivation. Female cannabis plants produce inflorescences that contain bracts densely covered by glandular trichomes, which synthesize a range of commercially important cannabinoids (e.g., THC, CBD) as well as terpenes. Cannabinoid content and quality varies over the 8-week flowering period to such an extent that the time of harvest can significantly impact product quality. Cannabis flower maturation is accompanied by a transition in the color of trichome heads that progresses from clear to milky to brown (amber) and can be seen visually using low magnification. However, the importance of this transition as it impacts quality and describes maturity has never been investigated. To establish a relationship between trichome maturation and trichome head color changes (phenotype), we developed a novel automatic trichome gland analysis pipeline using deep learning. We first collected a macro-photography dataset based on 4 commercially grown cannabis strains, namely 'Afghan Kush', 'Green Death Bubba', 'Pink Kush', and 'White Rhino'. Images were obtained in two modalities: conventional macroscopic light photography and macroscopic UV induced fluorescence. We then implemented a pipeline where the clear-milky-brown heuristic was injected into the algorithm to quantify trichome phenotype progression during the 8-week flowering period. A series of clear, milky, and brown phenotype curves were recorded for each strain over the flowering period that were validated as indicators of trichome maturation and corresponded to previously described parameters of trichome development, such as trichome gland head diameter and stalk elongation. We also derived morphological metrics describing trichome gland geometry from deep learning segmentation predictions that profiled trichome maturation over the flowering period. We observed that mature and senescing trichomes displayed fluorescent properties that were reflected in the clear, milky, and brown phenotypes. Our method was validated by two experiments where factors affecting trichome quality and flower development were imposed and the effects were then quantified using the deep learning pipeline. Our results indicate the feasibility of automated trichome analysis as a method to evaluate the maturation of female flowers cultivated in a highly variable environment, regardless of strain. These findings have broad applicability in a growing industry in which cannabis flower quality is receiving increased circumspection for medicinal and recreational uses.

1. Introduction

Cannabis (*Cannabis sativa* L.) is valued for its medicinal use in every continent except Antarctica, and many countries have established the

legal framework for the cultivation and sale of recreational cannabis derived products [1]. Drug-producing cannabis strains are characterized by large female inflorescences (flowers) that bear a cluster of pistils surrounded by bracts, which produce large numbers of glandular

Abbreviations: ADT, Average distance to the nearest trichome; DAF, Days after flowering; CF, Clumping fraction; NN, Nearest neighbor; PAR, Photosynthetically active radiation; CBD, cannabidiol; CBG, cannabigerol; CBN, cannabinol; THC, tetrahydrocannabinol; (CBD/CBG/CBN/THC)A, acid form of cannabinoid.

* Corresponding author.

E-mail address: darrens@sfu.ca (D.B. Sutton).

<https://doi.org/10.1016/j.atech.2022.100111>

Received 25 May 2022; Received in revised form 13 August 2022; Accepted 22 August 2022

Available online 28 August 2022

2772-3755/© 2022 The Author(s). Published by Elsevier B.V. This is an open access article under the CC BY-NC-ND license (<http://creativecommons.org/licenses/by-nc-nd/4.0/>).

trichomes where cannabinoids and terpenes are synthesized [2]. Cannabis plants require approximately 8 weeks to mature prior to harvest, after which inflorescences are dried for sale in their natural form or processed for value-added products (edibles, cosmetics, extracted oils). In order to ensure optimal cannabis quality, it is imperative to identify the stage at which the inflorescences are at the point of prime maturation and hence potency. There are currently no scientifically based methods to predict maturation and consequently harvests are performed on a calendar basis i.e. when plants have attained 7–8 weeks of growth. Methods to assess trichome maturation can lead to improvements in quality assurance for the cannabis industry.

In this work, we study cannabis trichome gland head phenotypes as flowers mature and visual trichome changes occur, such as a progression in color of the heads of trichomes from clear to milky to brown. Although these phenotypes have been suggested as a visual heuristic for harvest timing, little scientific work describes them during flower development and trichome maturation. Previous work supports the idea that browning of trichome heads is associated with quality degradation in dried cannabis [3], but the shelf life of dried cannabis [4] and progressive trichome browning in storage makes extrapolation of results to fresh cannabis tissue unpredictable. In order to understand the role of trichome phenotypes during trichome maturation, it is necessary to obtain measurements *in situ* during flower development.

We describe an automatic computational method that was built to extract trichome phenotype and morphology metrics during cannabis flower development from macroscopic photographs. To reduce uncertainty related to the chronology of observations, our method was implemented in a commercial greenhouse such that the time delay between excision and photography was minimized. By implementing recent advances in computer vision, we show our automatic method can be used to define trichome maturation in multiple cannabis strains in high throughput applications without repeated fine tuning.

2. Related work

2.1. Morphology of cannabis trichomes

Trichomes are ubiquitous structures in the plant kingdom. Many essential oil-bearing plants possess glandular trichomes that have important commercial value [5]. Trichomes can also consist of plant hairs lacking a gland, with a spike like appearance [6]. In hemp and drug-producing cannabis plants, Hammond and Mahlberg [7] studied trichome types using scanning electron microscopy (SEM) and described 3 types: bulbous, sessile, and capitate stalked. They subsequently described the morphological development of capitate stalked trichomes, observing stalk elongation and resin accumulation in the gland on top of the secretory cells [8]. These contributions laid the groundwork for the understanding of cannabinoid synthesis and storage *in planta*. Mahlberg and Kim [9] further characterized the formation of the trichome gland cuticle and proposed a working model of cannabinoid biosynthesis, hypothesizing that tetrahydrocannabinolic acid (THCA) is formed outside of plant cells in the storage cavity of the trichome gland [10]. Sirikantaramas et al. [11] confirmed this hypothesis by localizing the enzymes necessary for cannabinoid synthesis to the storage cavity, determining that cannabinoids are formed from a ring of secretory cells. Livingston et al. [12] further characterized the development of cannabis trichomes and observed that capitate stalked trichomes develop from sessile type trichomes during the flowering period. The development of trichomes from the sessile to cannabinoid rich capitate stalked type was accompanied by a shift in autofluorescence of the gland contents from green to blue.

2.2. Trichome maturation

The color transition of trichome heads from clear to milky to brown is often used to manually approximate the stage of maturation, with

milky representing the optimal state and brown indicating over-maturation [10,13]. However, the relationship between trichome head color and cannabis flower development has not been previously investigated. Previous work has shown a possible negative correlation between trichome head browning and cannabinoid content. Turner et al. [14] were the first to show reduced cannabinoid content in senescent (brown) capitate stalked glands, although statistical analysis was not reported. Cannabis samples acquired from law enforcement and manually assessed for trichome browning on a linear scale had a lower THCA and increased cannabinolic acid (CBNA) content compared to cannabis samples with clear or milky trichomes [3]. Reduced THC content in senescent trichomes glands was also reported by Mahlberg and Kim [10]. There is currently a lack of prior reports describing trichome gland phenotype in relationship to cannabis flower development *in situ* in cannabis.

2.3. Automatic assessment of plant trichomes

The microscopic nature of trichomes complicates manual observation, but recent advances in automatic methods to assess trichomes have enabled increasingly powerful analyses. Glandular trichomes of tomato were sorted by autofluorescent flow cytometry to separate young and mature trichomes prior to transcriptome analysis of the gland contents [15]. Failmezger et al. [16] estimated the 3D leaf surface of *Arabidopsis thaliana* from 2D microscopy image stacks to characterize trichome growth patterns. Mirnezami et al. [17] investigated image processing to automatically count soybean trichomes from microscopy images. Deep learning has also been applied to trichome analysis to estimate the 'hairiness' of cotton leaves as a metric of harvest readiness [18]. No previous studies have assessed trichome maturation in cannabis using these or similar approaches; thus, metrics that could be used to predict when cannabis inflorescences have achieved a maturation stage indicative of optimal cannabinoid content have not been established.

2.4. Contributions

In this work, we document changes in trichome gland head phenotypes over the flowering period and compare observations of the trichome glands and the supporting bract tissue. We present a computer vision pipeline to automatically segment and classify trichome gland head phenotypes and validate the pipeline by experiments that induce trichome degradation and alter trichome development. We also explore novel fluorescent trichome gland head traits induced under UV irradiation that were observed from whole glands, as opposed to previous studies that explore fluorescence in a confocal manner [12,31]. We acquired data using conventional optics such that our analysis was carried out *in situ* and yielded same day results. We discuss our results in the context of trichome development and cannabis flower maturation in four cannabis strains (genotypes) and conclude with comments on the feasibility of on-site imaging technology to automate quality aspects during the cannabis cultivation process in the greenhouse. In the following sections, we first describe plant materials, plant propagation, and computational analysis (Sections 3 and 4 respectively), then present results (Section 5) and conclude with the interpretation of results in the discussion (Section 6).

3. Materials and methods

3.1. Plant materials

This research was conducted in a Health Canada approved facility in which the plants were grown in a commercial greenhouse using a hydroponic method of cultivation. There were four strains (genotypes) studied that were grown during the winter months (October-April 2021, strains Pink Kush 'PK', and White Rhino 'WR') or during the summer months (May-September 2020, strains Afghan Kush 'AK', and Green

Death Bubba 'GDB'). During the winter period, plants were provided with supplementary lighting to achieve 1600 $\mu\text{Ein}/\text{m}^2$ of photosynthetically active radiation (PAR) using sodium lamps emitting a wavelength centered at 590 nm. During the summer period, supplementary lighting was provided where needed on overcast days to achieve the required PAR.

All plants were initiated from cuttings taken from stock (mother) plants of the four strains. The cuttings were dipped in rooting powder (containing indoleacetic acid) and inserted into 2.5 cm rockwool cubes, which were placed in trays in a propagation room under high relative humidity (80%) and a temperature range of 23–27 °C. After 2 weeks, when cuttings had rooted, they were placed into wells cut into 10 cm³ rockwool blocks and placed on a greenhouse bench for an additional 2 weeks to acclimatize and resume vegetative growth. Following this, they were transferred into large cocofibre blocks, one plant per block, and placed in a large flowering room where the photoperiod was adjusted to 12 hr lighting and 12 hr darkness to induce flowering. The water and nutrient regimes were adjusted according to commercial growing requirements to ensure adequate growth. The bags were arranged in rows, with 2 rows parallel to each other, and spacing of 0.5 m between plants. The plants were trained and supported by wire mesh netting that allowed the developing inflorescences to grow upright. Pruning of leaves and training of plants were conducted according to commercial growing requirements.

For experimental observations where inflorescences were photographed, each row of plants in the flowering room was divided into 10 zones, each containing up to 10 plants for observation such that no inflorescence was excised from the same plant twice. The zones were located in the center of the greenhouse to ensure uniform growing conditions. Plants were not treated with any foliar sprays that could influence trichome development. However, for one group of plants, a spray of potassium bicarbonate (Milstop) was applied to cannabis flowers of strain PK. Two plants each were sprayed with 100 ml of 2.5 g/L Milstop at 5 weeks and 6 weeks after flowering using a hand-held sprayer. Two control plants were misted with water. Images were collected the following week (flowering week 7) from these plants. For segmentation validation, plants from strain PK which were visually stunted due to infection by a viroid disease were compared to healthy plants. Images were collected from a stunted plant and two healthy control plants at flowering week 7.

3.2. Data collection

Images of inflorescences were obtained from plants that were in the 3rd to 9th week of flowering. Images were collected weekly from the onset of visible trichomes (week 3) to flower senescence (weeks 8 or 9, depending on strain). The inflorescences selected for photography were situated on the terminal apical branches of plants. Individual buds were carefully removed using pruning shears and transported to a designated room for image collection. The individual buds were separated into segments representing apical, mid and bottom regions and bract tissue samples were selected from both sides (Fig. 1). To capture the images of trichomes, both visible lighting (range of 400–700 nm provide by fluorescent lamps) and ultraviolet (centered at 350 nm) were used. The latter was achieved by using Baader UV-pass filters as described in Section 3.3. Each image was labelled according to location of the flower sample, day of the flowering period, cannabis strain, and illumination source. The dataset consisted of 840, 840, 720, and 720 images of strains PK, WR, AK and GDB, respectively. The former two strains were observed for an additional week to capture trichome browning. Image resolution was 6240×4160.

3.3. Image collection by photography

All photographs were captured with a Canon 6D Mk. II DSLR Camera (Canon, JP) fitted with a Canon MP-E 65 mm 1–5x macroscopic lens



Fig. 1. Flower dissection for photography. Cannabis inflorescences were photographed by morphology: Bract tissue from ① both sides of the apical floret, ② each of the opposite mid florets, and ③ each of the opposite basal florets was excised and photographed.

(Fig. 2). Camera configuration was as follows: Lens magnification 3x macro, f-number 16:14 conventional:fluorescent, color temperature 5500 K, sRGB color space, and exposure time of 1 s for both modalities. The camera was mounted on a table with vibration damping grommets. For UV excitation to photograph autofluorescence, a modified Vivitar 283 xenon flash (Vivitar, Santa Monica USA) had the stock Fresnel lens replaced with a Baader UV-pass filter (Baader-Planetarium, Munich DE) resulting in a flash centered at 350 nm and with a 60 nm bandwidth (320 – 380 nm). The single-photon fluorescence excitation wavelength of ~350 nm used in this study is approximately equivalent to the two-photo excitation wavelength of 720 nm used by Livingston et al. [12] to characterize the fluorescence of sessile and capitate stalked trichomes of hemp. Our approach uses simpler optics such that the camera prototype can be dismantled and redeployed rapidly *in situ*, and the chosen fluorescence excitation wavelength is outside of the spectral sensitivity of most conventional image sensors. The Vivitar flash was synchronized to the Canon DSLR camera via Elinchrom wireless flash trigger. All images were captured with a color calibration swatch in view, and fluorescent images were captured under conditions of complete darkness.

4. Machine learning methods

4.1. Trichome gland segmentation

Observations were made of trichome glands (Fig. 3) that formed on the surfaces of bract tissues. Trichome glands were often partially occluded or stuck to other trichomes, complicating the segmentation of individual gland instances. Instance segmentation is a difficult problem in computer vision because it requires the algorithm to separate the foreground from the background in the image *and* individual components (trichome glands) of the foreground scene. We used the deep learning neural network 'DO-U-Net' [19] designed for instance segmentation of repeated convex shapes in 2D microscopy and aerial images, where a dual decoder U-Net architecture predicts a semantic mask describing foreground membership (trichome glands), and the edges of each trichome gland in the image (Fig. 4).

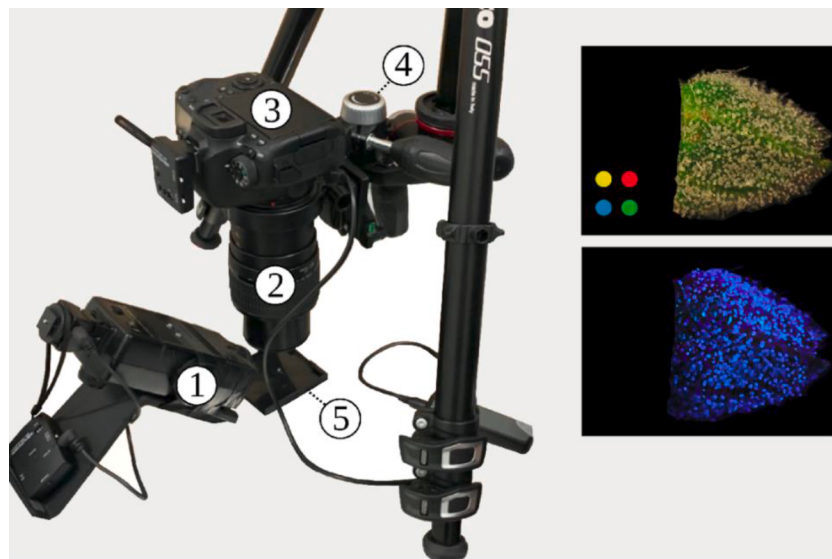


Fig. 2. The image collection prototype. Left: ① A modified Vivitar xenon flash, emitting a ~50 nm wide spectrum centered at 350 nm, ② Canon MP-E 65 mm macro lens, ③ Canon 6D mk. II DSLR camera, ④ Manfrotto adjustable tripod, ⑤ photo plate with color calibration. Right: Images captured using light (top) and UV induced fluorescence of bract tissues.



Fig. 3. COLOR FIGURE Images of bract tissues from the dataset. Conventional (bottom row) and paired auto-fluorescent images (top row) of strain 'PK' at (left to right): 3, 5, 7 and 9 weeks of flowering. Scale bar represents 1 mm.

DO-U-Net achieves instance segmentation by subtracting the predicted edges of trichome glands from the trichome gland mask, such that individual glands are isolated. We apply the same loss function and training parameters as outlined in the DO-U-Net method, only making minor adjustments to edge and mask post processing such that adjacent trichome glands are separated by single pixel width lines. We noted that the original implementation of DO-U-Net tends to shrink the size of detected trichome glands due to the edge subtraction operation, thus we incorporated a custom post processing method using Voronoi cells to mitigate this effect (Fig. A2, appendix). The DO-U-Net training and testing data was a manually annotated subset of the data described in Section 3.2, consisting of 156 (136:20 training:testing) images drawn uniformly with respect to strain and observation time to construct a balanced segmentation dataset (Fig. A1, appendix). We implemented

DO-U-Net in PyTorch, using the built in ADAM optimizer. To ensure the network generalized well to unseen data, we augmented the inputs at training time using standard augmentation procedures: random horizontal or vertical flipping, random rotation, and random color jitter. Training time was approximately 2 h and was terminated after 100 epochs running on a Nvidia 1080ti GPU with 12 GB memory. The network was trained on 512×512 pixel image patches randomly cropped from input images. At inference, output mask patches and edge patches were stitched back together to compute mask and edge predictions for whole bract tissue images, followed by application of our post processing procedure. We refer the reader to the appendix where supplementary figures describe the post processing steps in detail.

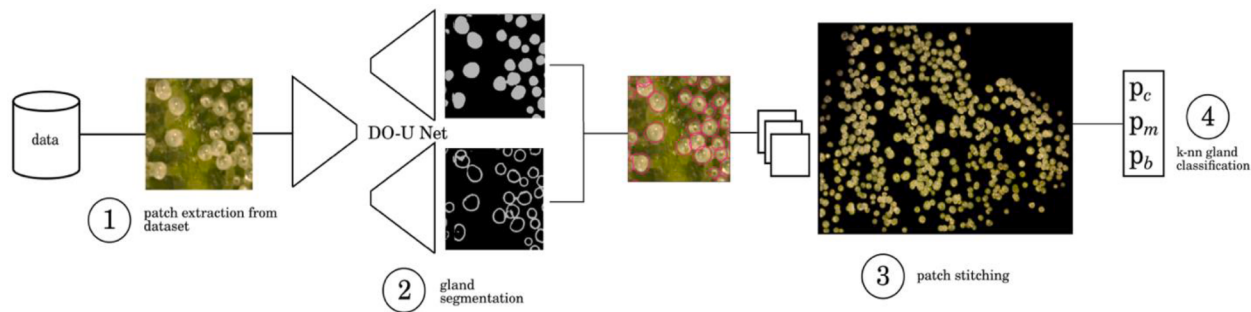


Fig. 4. COLOR FIGURE Segmentation pipeline. Input image patches ① are segmented into trichome glands ② using the artificial neural network DO-U-Net. Outputs from different patches are stitched together ③ to segment trichome gland instances for each image. ④ Glands are then individually classified by phenotype using a k-nn classifier (Fig. 5).

4.2. Trichome phenotype classification

A k-NN classifier was trained on manually labeled trichome glands (Fig. 5). For each strain, 10 glands from the classes representing 'clear', 'milky', and 'brown' were delineated manually. Each segmented gland was transformed from the sRGB to the CIELAB color space to disentangle color from luminosity, reducing the effect of shadows on classifier accuracy. Features were extracted by taking the mean of the L, a, and b color channels, and the mean of a hessian (H) filter applied to the chroma

$$c = \sqrt{a^2 + b^2} \quad (1)$$

The hessian filter is responsive to fine lines and details observed in clear trichomes but obscured in milky trichomes. For inference, k was set to 5, and the votes of training points were weighted by inverse distance. The mean and standard deviation calculated from the training data were applied to test data to standardize features at inference.

4.3. Analysis of trichome morphology

Changes in trichome morphology were assessed by computing metrics describing connected components in the post-processed semantic segmentation maps predicted by the DO-U-Net. Connected components are groups of contiguous foreground pixels representing a trichome head gland. The average distance to the nearest trichome gland (ADT), trichome gland density (trichome glands per mm²), trichome diameter (in microns), trichome clumping fraction (CF), and roundness were computed from the data for each strain and phenotype where phenotype specific metrics were meaningful. The ADT was calculated as the mean of the distance transform describing the average distance to the nearest trichome gland over the area of the bract tissue. Trichome density was computed by counting the number of trichome instances and dividing by the pixel area of the bract tissue, then scaling by the spatial pixel size of 2 µm. Trichome diameter was computed as the diameter of a disk with the

equivalent pixel area to each trichome gland instance. CF was calculated by comparing the number of trichome gland instances detected in each bract image when connectivity was defined as 4 pixel or 8 pixel. In other words, trichome gland instances that were delineated by a single pixel line after post processing were deemed separate by 4-connectivity but connected by 8-connectivity. A comparison of the two trichome gland counts indicated how many trichomes were clumped together in the image. The CF is expressed as:

$$\frac{(N_4 - N_8)}{N_4} \quad (2)$$

for each image where N is the number of trichome instances detected by the connectivity denoted by the subscript (Fig. A3, Appendix). Roundness was calculated by the circularity metric

$$4\pi \cdot \frac{A_{gland}}{Perimeter_{gland}^2}. \quad (3)$$

4.4. Statistical analysis

Data were subjected to independent two-sided T-tests for significance in validation experiments (Milstop and disease induced stunting) at $p < 0.05$. For trichome head diameter results and the morphological metrics ADT, density, CF, and roundness, the Seaborn plotting library visualized means, standard deviations of the mean, and first or second order regression lines. For regression lines, the 95% confidence intervals of trend lines were visualized to assess whether the confidence intervals of the trend lines overlapped (Figs. 8 and 15). Confidence intervals that did not overlap were interpreted as being trendlines of significantly different groups.

4.5. Validation

We validated our algorithm using a hybrid approach, combining

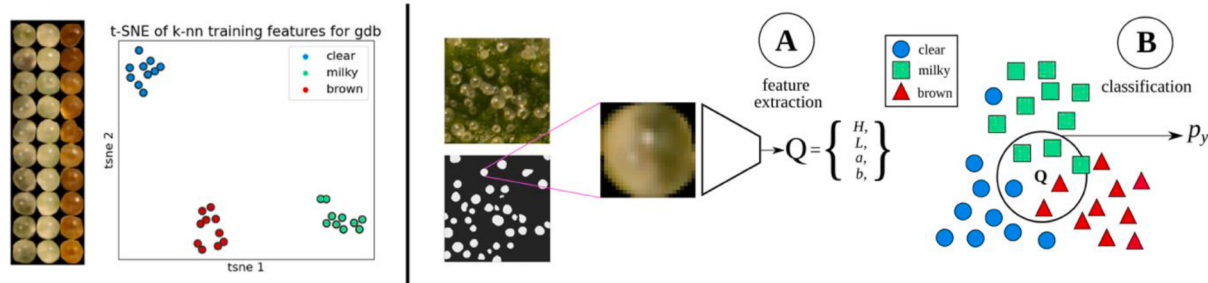


Fig. 5. COLOR FIGURE k-NN classifier. Left: Ten clear, milky, and brown trichomes (gland columns 1-3 respectively) used to train the k-NN classifier for strain GDB, and the resulting t-SNE clustering of training features. Right: At inference, the k-NN classifier ④ extracts features and ④ predicts the probability of each gland instance belonging to class clear, milky, brown. A k-NN classifier is constructed for each strain, here we only show the classifier for GDB for brevity.

manual assessment of gland segmentation and classification accuracy, and experimental assessment of algorithm predictions compared to prior biological knowledge of the cannabis flower. Pixelwise metrics, although useful for determining performance discrepancies between automatic methods, have less meaning when assessing the performance of an algorithm in the context of the biological domain being investigated. Therefore, we turn to the recommendation of Sbalzarini [20] who argued that the most pragmatic method of validating a bio-imaging algorithm is to test predictions against prior knowledge from the same domain as the research question. We conducted two validation experiments, the detection of stunted trichome maturation as predicted by trichome diameter when flowers were subjected to viroid disease stress, and the detection of trichome browning when flowers were sprayed with an alkaline chemical treatment (Section 3.1).

5. Results

We manually inspected the accuracy of the predicted segmentation masks on a withheld test set of bract images. We observed a low false positive rate and satisfactory instance segmentation of whole trichome gland heads (Fig. 6). Glands that detached from stalks and released their contents to form amorphous blobs of resin were not detected. The accuracy of the k-NN classifier was verified via manual assessment of bract tissue images at different flowering time points to confirm trichome head phenotype predictions correctly described trichome gland development from transparent sessile and pre-stalked capitate (clear) to capitate stalked abundance (milky) prior to harvest time until trichome gland senescence (brown).

An examination of the clear-milky-brown results of all four cannabis strains over flowering time showed that in general, trichome browning was absent until approximately 50 days after flowering (daf) (Fig. 7). There was a rapid increase in the prevalence of brown trichome heads at 65–75 days of the flowering period. By comparison, the clear trichome heads were most abundant at day 25 of the flowering period, and began to steadily decline up to the end of the experiment (harvest time, day 65–75 of the flowering period, depending on the strain). The trichome heads displaying the milky phenotype began to gradually increase in prevalence in each strain, with a peak at day 55 in PK, at day 50 in

strains AK and GDB, and a maximum at day 70 in WR. A significant difference in trichome gland head phenotype was not observed when assessed by dissection morphology as outlined in Fig. 3.

The changes in trichome head diameter over the flowering period are shown in Fig. 8. For all strains, there was a gradual increase in diameter up to around day 50, coinciding with the emergence of the brown phenotype. Gland head diameters steadily decreased following the onset of trichome browning. The head diameters of brown trichomes were consistently smaller for all four strains, ranging in size from 75 to 85 µm (strains PK and WR) and 85–95 µm (strains AK and GDB). In general, diameters of milky trichome heads were greater than clear (strains AK and GDB) or the same (strains PK and WR), with peak sizes of 105–110 µm (AK, GDB) and 95–100 µm (PK, WR). The average trichome head diameter of clear trichomes peaked at approximately the same size as the milky phenotype for strains PK and WR and at a diameter of 100 µm for strains AK and GDB. The ADT increased for strains PK, AK, and GDB, related to an expansion of bract tissue during the flowering period, whereas WR showed a slight reduction in ADT that corresponded to a delayed milky phenotype peak and stunted growth relative to other strains in the experiment (Fig. 9). In general, trichome gland heads diverged from bract venation to form stripe like groupings of trichome heads aligned axially with the supporting bract tissue during the mid to later stages of flower maturity. This stripe pattern was caused by stalk elongation normal to the concave surface of the abaxial bract tissue, exposing venation and surrounding non glandular tissue to direct sunlight. When trichome gland prevalence was expressed as density (trichomes per mm², Fig. 10), there was a steady decline over time in the flowering period for all four strains, with PK and WR sustaining a higher density at harvest of 25–30 trichomes/mm² compared to AK and GDB at 20–25 trichomes/mm², corresponding to non-glandular bract tissue expansion, increased stalk length, and trichome gland striping. The reduction in estimated density of trichomes could also be explained by the decreasing trend of trichomes that clumped together (Fig. 11) in strains AK and GDB, whereas strains PK and WR displayed a flat and increasing trend in CF over the flowering period and retained higher trichome densities. Importantly, PK, AK and GDB displayed higher average CF (i.e., a higher clumping curve offset) over the flowering period compared WR, corresponding to the arrested trichome

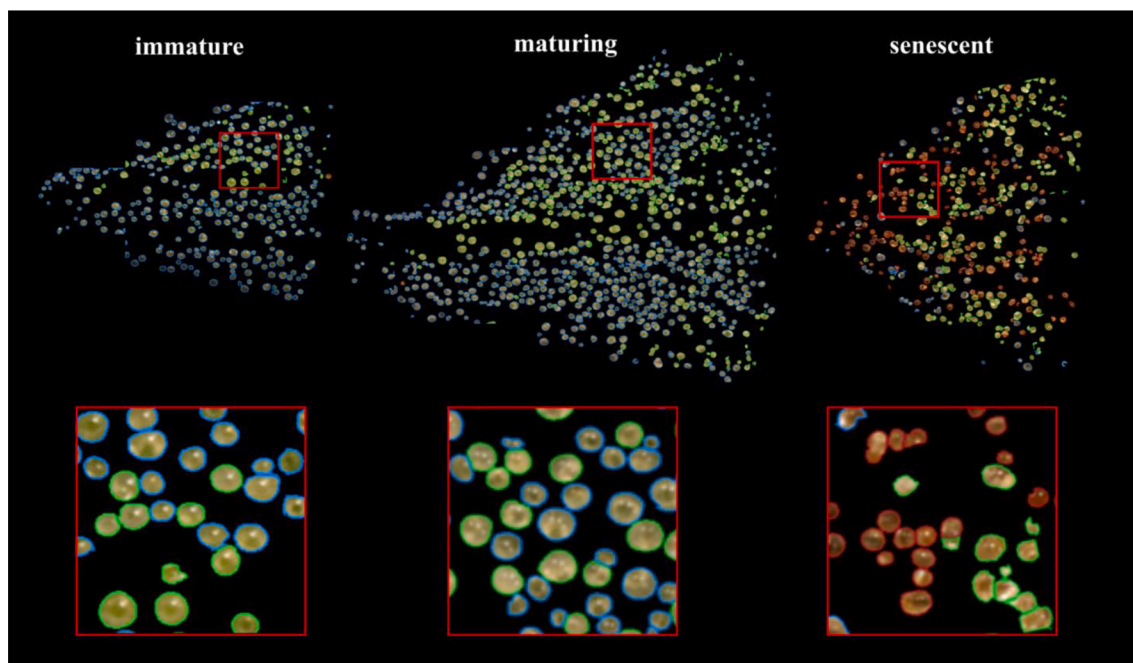


Fig. 6. COLOR FIGURE Segmented and classified trichomes glands. Top to bottom: immature, mature and senescent bract tissue of strain PK. Glands are circled according to their classification: clear (blue), milky (green), or brown (red). Zoomed in patches show detailed segmentation and classification results.

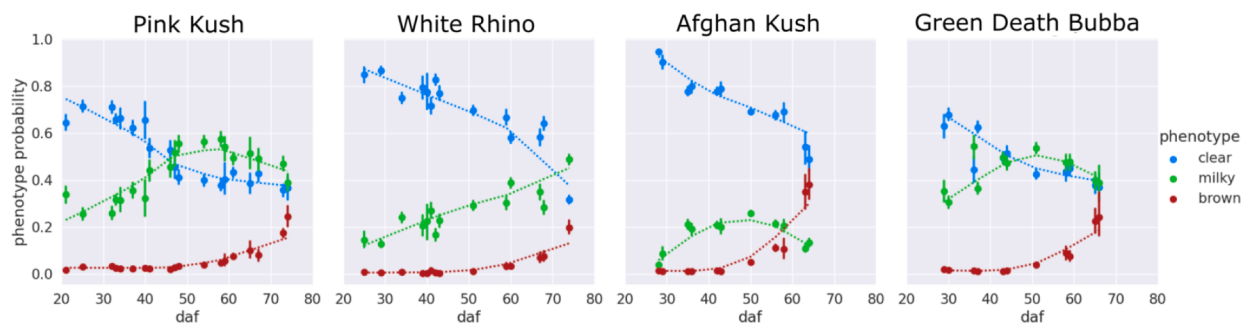


Fig. 7. COLOR FIGURE Clear, milky, brown phenotype probability. Local regression trend lines (dotted) of clear (blue), milky (green) and brown (red) phenotype probability. Points are means of the observed trichomes, with error bars showing the standard deviation of the mean. Results should be interpreted as the probability of a randomly chosen trichome, observed at a time during the flowering period, belonging to a phenotype class clear, milky, or brown. Local regression lines are for visualizing the phenotype trend over the flowering period.

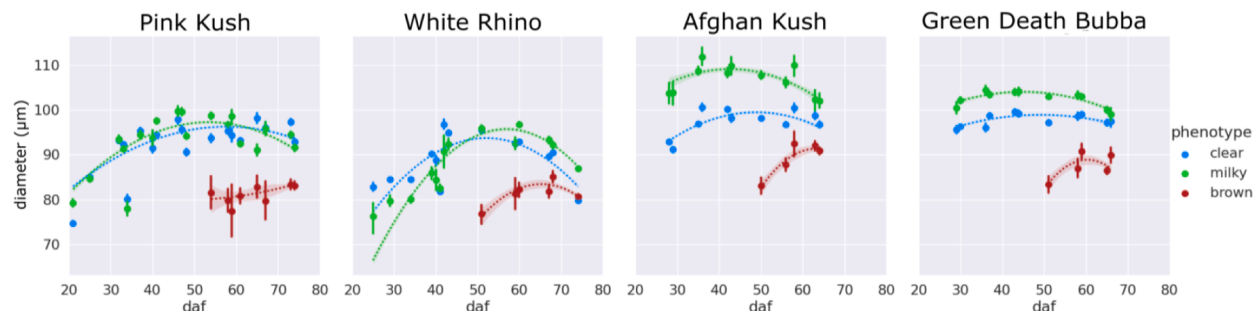


Fig. 8. COLOR FIGURE Trichome diameter. For each phenotype observed over the flowering period, trichome gland head diameters were computed. Points are the mean of all trichomes observed and error bars correspond to the standard deviation of the mean. Second order regression lines fitted to each phenotype display 95% confidence intervals as transparent bands.

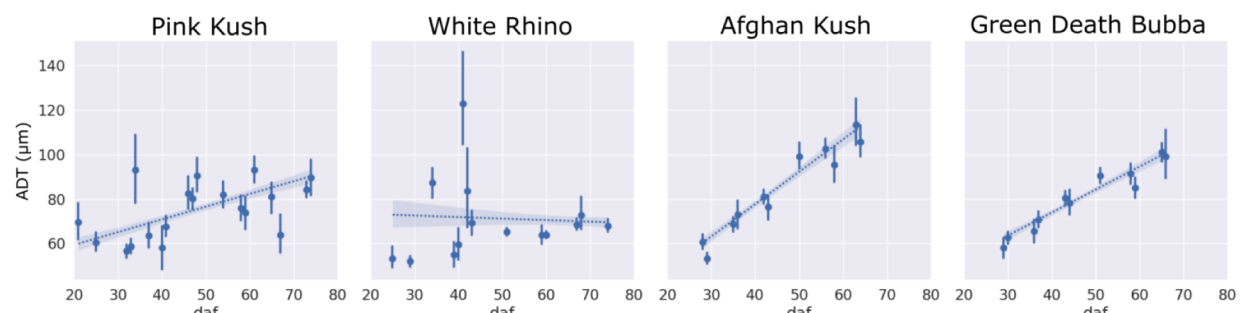


Fig. 9. Average distance to the nearest trichome (ADT). For each photographed bract image, the average distance to the nearest trichome was computed. Points are the mean of all bract tissue samples observed, with error bars representing the standard deviation of the mean. Linear regression lines display 95% confidence intervals as transparent bands.

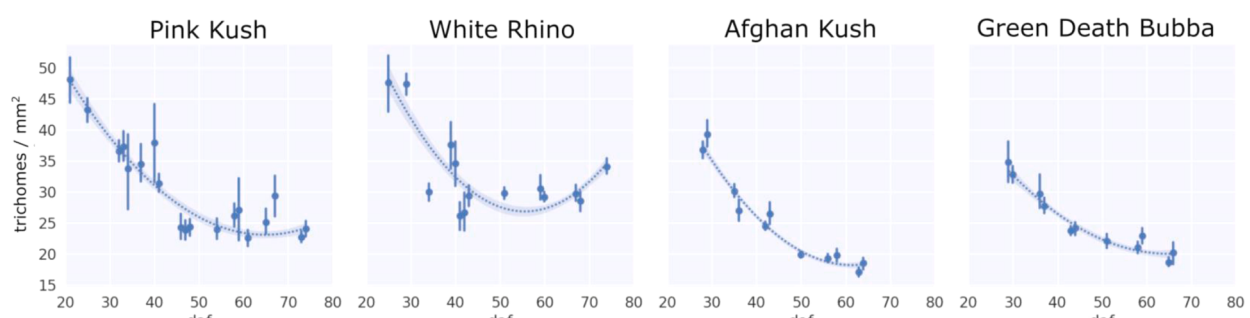


Fig. 10. Trichome density. For each photographed bract image, trichome density was computed as the number of trichome gland heads per square millimeter. Points are the mean of all bract tissue samples observed at the specified flowering time, with error bars representing the standard deviation of the mean. Second order regression lines display 95% confidence intervals as transparent bands.

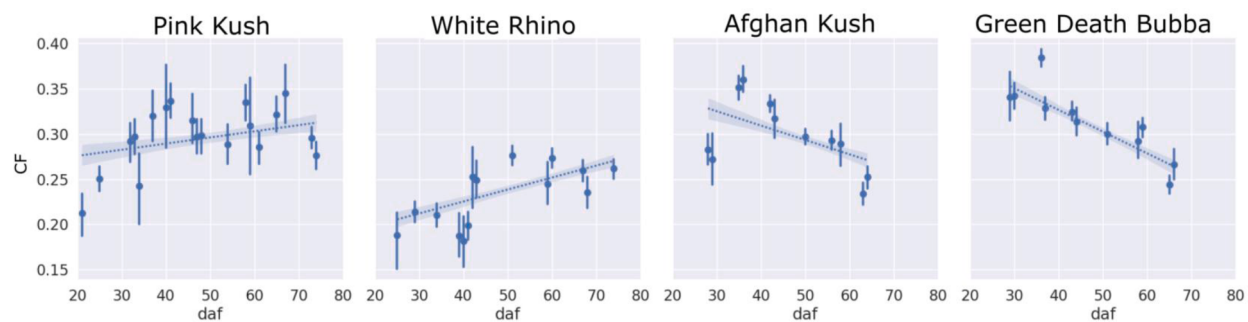


Fig. 11. Clumping fraction (CF). For each photographed bract image, the clumping fraction was computed as the relative difference in detected trichome glands using different connectivity criteria (Eq. (2)) observed over the flowering period. Points are the mean of all bract tissue samples observed at the specified flowering time, with error bars representing the standard deviation of the mean. Linear regression lines display 95% confidence intervals as transparent bands.

development that can be visualized by inspecting stalk development of WR trichomes (Fig. 12). The clumping of trichome heads could be readily visualized when examined under a scanning electron microscope (Fig. 13). Trichome roundness as assessed by the circularity metric reduced steadily for all four strains over the flowering period, related to the degradation of trichome gland heads and changes in camera view due to trichome stalks elongating in plane and turning trichome heads to side with respect to the camera (Fig. 14).

When the UV induced autofluorescence was examined over the time of the flowering period, there was a peak in the fluorescence color angle as parameterized by the CIELAB a-b color space at approximately 40 days of the flowering period followed by a decline (red shift) in all four strains observed. The decline was gradual in trichome heads showing a clear or milky phenotype and much more pronounced in the brown trichome heads (Fig. 15), presumably due to differences in chemical composition of the fluorescing substance in brown trichomes compared to gland heads of the clear or milky phenotype. Brown trichomes had a more negative fluorescence color angle than clear or milky trichomes from onset of trichome browning until experiment end for all strains, fluorescing green-blue (Fig. 16). In general, fluorescence intensity increased over the flowering period (Fig. 17), indicating an accumulation of the fluorescent substance, likely cannabinoids.

The application of potassium bicarbonate (Milstop) to cannabis flowers increased trichome browning compared to the water treated control (Fig. 18) and red shifted the fluorescence color angle compared to the control (Fig. 19, top left), due to a higher number of brown trichomes observed in the treated tissue. Milstop application also reduced trichome density (Fig. 19, top right and Fig. 20) and clumping (Fig. 19, bottom right) due to degradation of the trichome head cuticle, but did not significantly affect the average distance between trichomes (Fig. 19, bottom left), as this metric is dominated by bract tissue expansion that was not affected by Milstop. Visually stunted plants that displayed signs of viroid disease (Fig. 21) due to arrested trichome development by

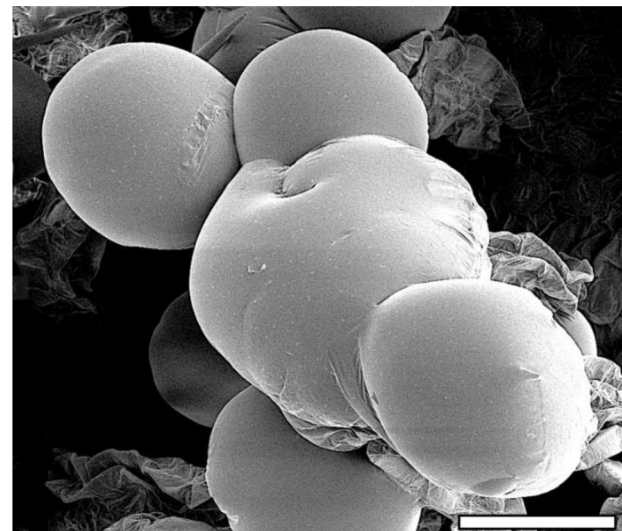


Fig. 13. Scanning electron microscopy image of clumped trichomes. Senescent flower tissue was imaged by cryogenic SEM to observe resin leakage from glands and gland clumping. Scale bar (lower right) represents 50 μ m.

presumed disease pressure, when assessed by our automatic pipeline showed significantly smaller trichome size, with the mode of the stunted group occurring at a diameter of approximately 80 μ m whereas healthy control plants possessed trichomes of approximately 100 μ m diameter (Fig. 22, left). The density between groups was not significantly different (Fig. 22, right), which indicated that the visual manifestation of disease induced stunting was mainly observed as arrested trichome development, a lack of capitate-stalked trichome type, and smaller flower mass.

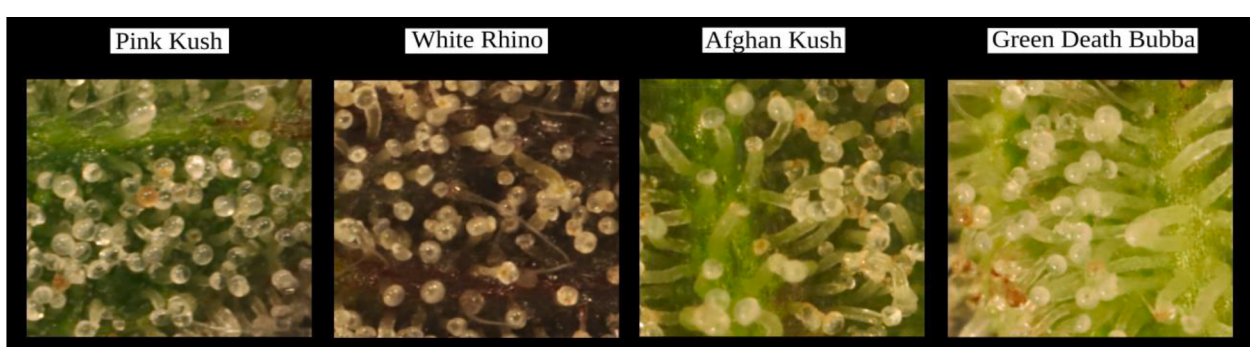


Fig. 12. Trichome stalk length. Left to right: Image patches of PK, WR, AK, and GDB flower tissue at harvest (flowering day 50). Strain WR displayed stunted glandular trichome stalk development compared to other strains.

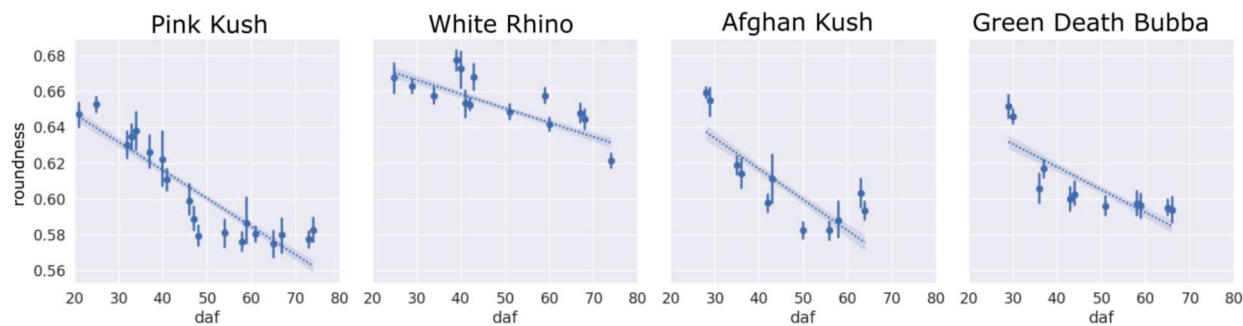


Fig. 14. Trichome gland head roundness. For each bract image, the circularity was computed as shown in Eq. (3). Points are the mean of all bract tissue samples observed at the specified flowering time, with error bars representing the standard deviation of the mean. Linear regression lines display 95% confidence intervals as transparent bands.

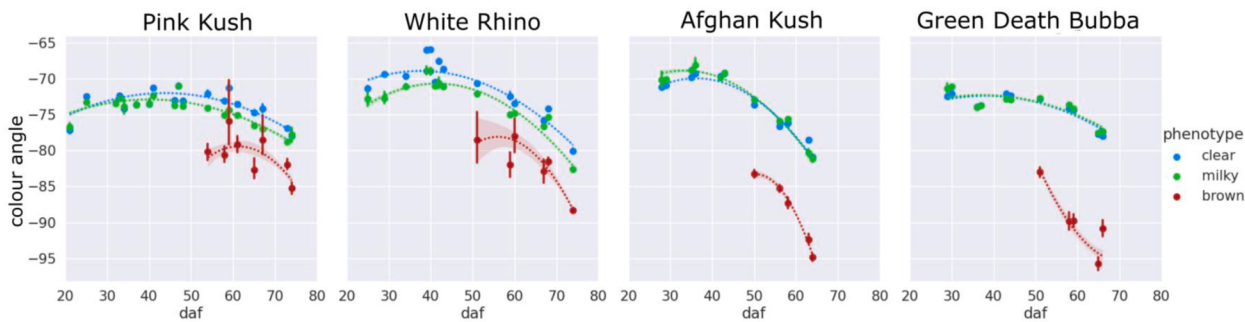


Fig. 15. COLOR FIGURE Trichome gland head fluorescence. The CIELAB color angle describing fluorescence spectra of for all trichome gland heads observed over the flowering period. Points represent the mean of all trichomes observed at the specified flowering time, with standard error bars representing the standard deviation of the mean. Second order regression lines fitted to each phenotype display 95% confidence intervals as transparent bands.

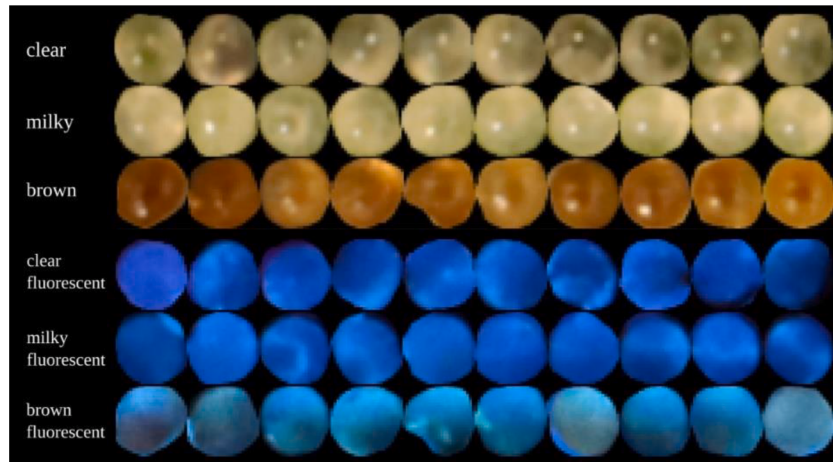


Fig. 16. COLOR FIGURE Trichome gland heads and corresponding fluorescence. Qualitative display of visual phenotype and corresponding trichome fluorescence of strain GDB. Rows, from top: clear trichome heads, milky trichome heads, brown trichome heads, fluorescing clear trichome heads, fluorescing milky trichome heads, fluorescing brown trichome heads. Note the red shift of brown trichome fluorescence.

6. Discussion

Cannabis trichomes display visual cues of maturation during flower development, but their small size obscures important aspects of their morphology and appearance to the unaided eye. Unlike other crops where visual observations can be relied upon to predict maturity and optimal harvest time, e.g., changes in fruit color and size, cannabis trichomes display maturity indicators at a microscopic scale, complicating visual inspection. In this case, obtaining visual patterns of trichome maturity requires a systematic approach that integrates recent advances in automatic computer vision supported by biological knowledge of the

cannabis plant. Prior to this study, there was no description of cannabis trichome maturation during flower development *in situ*, where data was collected as on-site images and results could translate directly to the cultivation process in the greenhouse. To achieve this, we reasoned that the visual trichome gland head phenotypes described as clear, milky, and brown, that previously were used as unconfirmed descriptors of trichome gland maturation [21], could be used to characterize trichome maturity when implemented as discriminating features in an automatic, data driven analysis of cannabis flower images. We used our automatic method to observe the evolution of visual trichome phenotypes and metrics describing changes in trichome morphology over the flowering

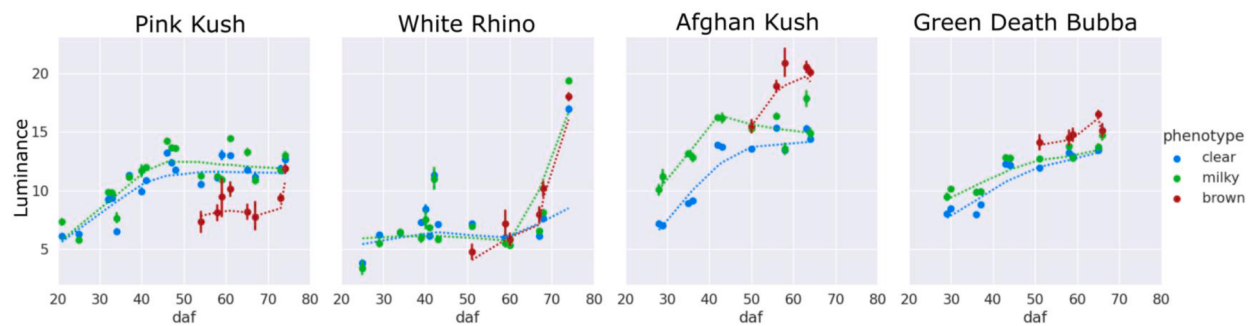


Fig. 17. COLOR FIGURE Trichome fluorescence luminosity. The L value from the CIELAB color space of fluorescing trichomes, describing fluorescent intensity but not spectrum. All phenotypes clear (blue), milky (green), and brown (red) show increasing average intensity with time, indicating an accumulation of the fluorescent substance. Local regression lines show qualitative trend over the flowering period.

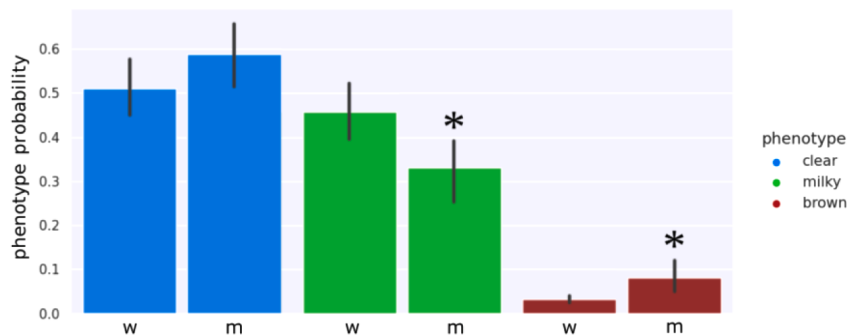


Fig. 18. COLOR FIGURE Milstop affects trichome gland head phenotype. Phenotype probability of water control (w) and Milstop treated (m) trichomes. Milstop treatment significantly increased trichome browning and reduced milkyness at $p < 0.05$, denoted by asterisks over the bars. The clear phenotype probability was not significantly different between groups.

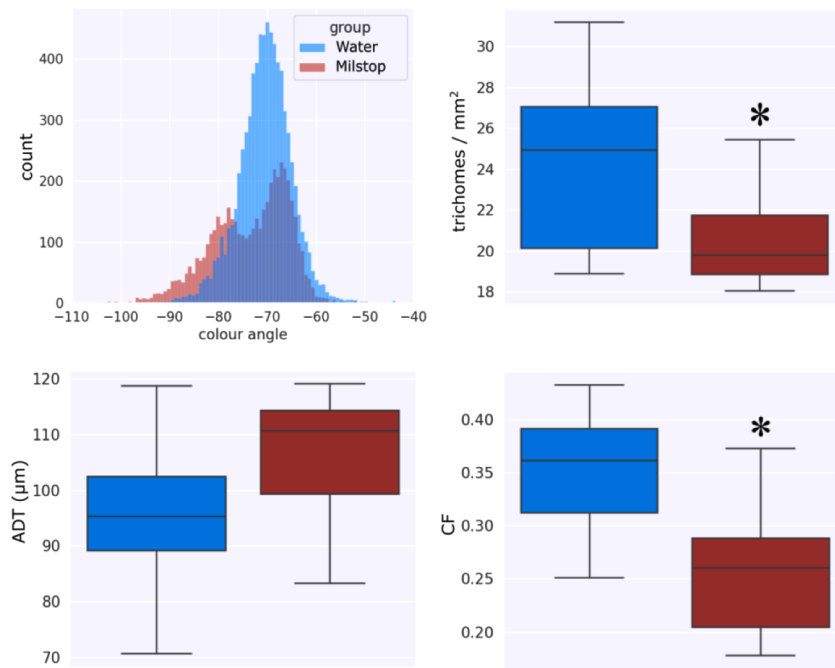


Fig. 19. Milstop application affects trichome morphology. Clockwise from top left: Fluorescence CIELAB color angle (greener color angles are more negative) of control and Milstop treated trichomes, distribution means are significantly different at $p < 0.01$, Milstop significantly reduces trichome density at $p < 0.05$, Milstop significantly reduces clumping factor at $p < 0.05$, Milstop does not significantly affect the distance to the nearest trichome.

period from developing flowers. We then compared these results to other morphological indicators of trichome maturity, specifically trichome gland head diameter and trichome stalk length. Our results

show that (1) trichome maturity can be described by trichome morphology metrics; (2) the temporal characteristics of the clear, milky, and brown phenotype curves validate their role as visual indicators of

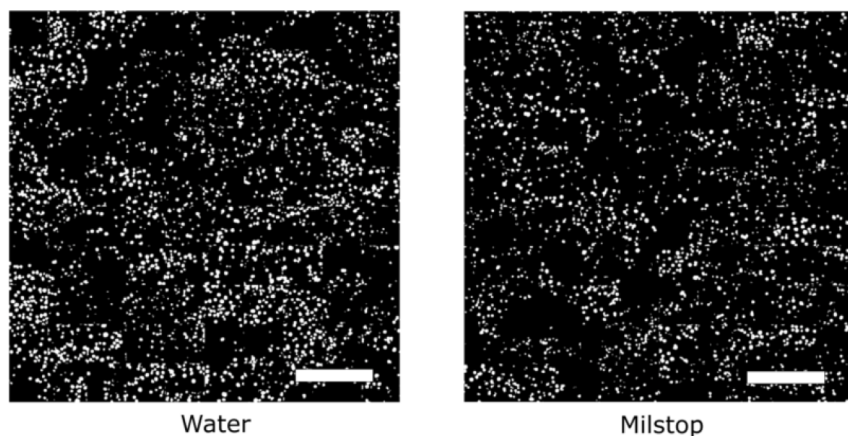


Fig. 20. Patches of DO-U-Net trichome gland segmentation. 100 patches from water treated control and Milstop treated trichomes showing the effects of the treatment on density and the CF metric. Scale bars represent 2 mm.



Fig. 21. Healthy (left) and viroid diseased (right) cannabis flowers of strain Pink Kush showing stunted development in the latter.

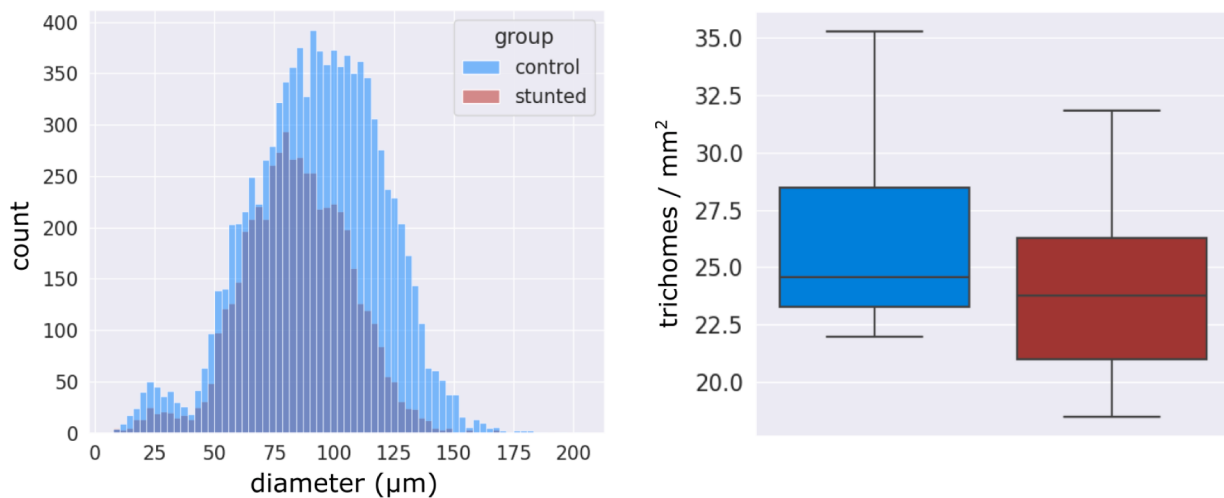


Fig. 22. Flower stunting affected trichome development. Left: Stunting from visually confirmed viroid disease reduces trichome diameter significantly at $p < 0.0001$. Healthy trichomes have a mode of 100 μm, compared to trichomes from stunted bract tissue with a mode diameter of approximately 80 μm, (Right) Stunting does not affect trichome density due to reduced flower tissue growth of the stunted group.

trichome maturity; (3) the clear, milky, and brown phenotypes can be differentiated by trichome gland head fluorescence, further validating their role as phenotypic markers of trichome maturity; and (4) changes in trichome gland head phenotypes and morphological metrics induced by chemical treatment and plant disease stress can be detected, thus validating our automatic method.

6.1. Morphology metrics describe trichome maturation

The biological processes that are associated with resin accumulation in cannabis strains have recently been explored by proteomic, genetic, and plant metabolic studies to understand cannabinoid synthesis and trichome maturation during cannabis flower development [21–23]. Our morphological characterization of trichome development concurs with these changes that describe cannabis flower development and trichome maturation at the cellular level. We describe factors such as temporal changes in distance to the nearest trichome, density, clumping fraction, and head roundness in concordance with stalk elongation, flower development, and trichome maturation.

6.1.1. ADT

The distance to the nearest trichome (ADT) metric described flower tissue expansion—a positive slope corresponded to healthy flower growth where bract tissue expanded at a faster rate compared to trichome diameter and presumably energy production (through photosynthesis) increased during the flowering period to support trichome maturation. Strains that did not show a positive increase in ADT (e.g., WR) subsequently displayed stunted trichome development i.e., small gland head diameter, arrested stalk elongation, and small flower size at harvest. This impact on WR is presumed to have been due to additional stress imposed on the plant through hermaphroditism (self-pollination), which arrests flower development and resin accumulation by diverting energy to pollen and subsequent seed formation [24,25]. The reliance of trichome maturation on flower development was reported by Conneely et al. [23], who exhaustively studied the protein expression of trichome head glands, stalks, and supporting bract flower tissue. They determined that bract tissue is important for starch synthesis through photosynthesis to fuel trichome development and cannabinoid biosynthesis during the flowering period, when the vegetative fan leaves begin to senesce.

6.1.2. CF

The clumping fraction (CF) morphology metric described a relationship between trichome diameter and bract tissue expansion. We note the symmetric relationship between the ADT and CF curves for all strains in this study, indicating these metrics are describing similar biological phenomena. Strains AK and GDB had large trichome diameters at the start of the experiment such that trichomes impinged against each other on underdeveloped bract tissue, and therefore had an increased CF compared to strains PK and WR. The CF for AK and GDB then decreased due to bract tissue expansion, indicative of healthy flower development over the flowering period. Conversely, the CF of WR increased over the flower period, starting from low initial CF caused by small sized trichomes on incipient bract tissue at the start of the experiment that did not impinge against each other, followed by a CF increase over the harvest period, indicative of trichome gland heads expanding at a faster rate than the underlying bract tissue.

6.1.3. Density

Lower trichome head density (trichome gland heads per mm² of bract tissue) at harvest, caused by bract tissue expansion during flower development, co-occurred visually with trichome stalk elongation, corresponding to previous studies that found the secondary metabolism of trichome gland heads required support from enlarged flower tissue [22, 23] and photosynthesizing stalks. In this study, we sampled the apical inflorescences, which are some of the largest of the plant. Recent work on the morphology of cannabis inflorescences found inflorescence width

to vary by more than a factor of 2 between the smallest and largest inflorescences at harvest [26], indicating that flower growth probably offsets the drop in trichome gland density we observed over the flowering period. The reduction in density we observed across all strains in the experiment has also been reported by manual counting of trichome gland heads observed under SEM modality, showing a decreasing density trend [27]. Interestingly, WR maintained the highest density over the flowering period, while AK and GDB achieved the lowest gland head density, indicating trichome glands per unit area of bract tissue decreased with flower development and trichome maturation. Another factor that could affect density measurements but not explored in this work is the detachment of trichome head glands from supporting stalks. This process presumably occurs when flower development reaches maturity, and especially at senescence.

6.1.4. Roundness

All strains showed a decrease in gland head circularity, as computed by Eq. (3). We attribute this to the degradation of the trichome head resulting in various shapes of trichome heads. WR showed the smallest decrease in circularity over the flowering period compared to other strains, indicating limited gland degradation that can also be observed by a lack of observed trichome browning.

6.1.5. Trichome morphology to profile trichome maturation

Strain PK displayed a profile of morphological metrics that was in between the extremes of the upper bound morphology metric profiles of AK and GDB, both of which displayed elongated trichome stalks at harvest time, and the lower bound profile of WR, where trichome stalk elongation did not occur and trichome gland head diameter was small. The trichome gland head diameter and stalk length observed in PK was also between the upper bound of AK and GDB, and lower bound of WR, indicating that our morphology metrics form a 4-dimensional description of trichome maturity. Furthermore, our morphological metrics infer a close relationship between trichome maturation and the development of the supporting flower, suggesting that trichome maturation only occurs if the supporting bract tissue expands. Bract tissue growth could be predicted by extrapolating the slope of observed morphology metrics, thus yielding a simple model to approximate flower maturation from image data.

6.2. Trichome phenotypes have distinct temporal curve characteristics

The trichome phenotypes clear, milky, and brown have little prior scientific evidence to substantiate their use as visual indicators of glandular trichome maturation, and subsequently their utility during the flower development process has not been adequately elucidated. Mahlberg and Kim reported that capitate-stalked trichome glands, when viewed under a stereomicroscope, were translucent during intense resin accumulation [10], and demonstrated that brown trichomes have a lower THC content. The reduced THC content of brown trichomes has also been observed in dried flowers [3].

6.2.1. Trichome phenotypes generalize to cannabis strains

Our results show a striking relationship of each phenotype during flower development. Strains AK, GDB, and PK that displayed stalk elongation and increased trichome diameter at harvest had a distinct peak in the occurrence of the milky phenotype over the flowering period, whereas this peak was absent for strain WR. All strains showed the clear phenotype dominating at the start of the experiment and followed a common trichome phenotype transition regardless of strain. Trichome phenotype response was affected by stress caused from changes in the growing environment, and the clear, milky, brown phenotypes appeared to be strain agnostic indicators of flower development.

6.2.2. Clear to milky transition

The clear to milky phenotype transition could be due to a mixing of

immiscible molecules in the trichome gland head during resin accumulation [9,10]. As cannabinoid precursors are secreted into the trichome gland head cavity by a disk of secretory cells at the base of the gland, superior to the stipe cells [12,28], vesicles distribute cuticle building molecules that enable the trichome head to continuously expand [10,29]. The migration of waxy cuticle precursors in vesicles into the gland head would result in an opaque gland head appearance due to the varying refractive indices of hydrophilic and hydrophobic substances obscuring the passage of light; thus, the visual transition from clear to milky likely indicates changes in amounts of cuticle-forming precursors and changes in the internal contents of the head [12,30]. Mahlberg and Kim [9] and Livingston et al. [30] showed that the waxy cuticle of mature stalked trichomes is significantly thicker compared to the sessile non-stalked type, which could also increase the opacity of the trichome head gland when viewed externally.

6.2.3. Trichome phenotype and flower maturity

There was a defined peak in the milky phenotype that occurred when trichome development was accompanied by stalk elongation to form the capitate-stalked trichomes [12]. In instances where a milky phenotype peak was not observed (e.g., in WR), stalk elongation was reduced, mean trichome diameter was smaller, as seen in non-drug producing trichomes of hemp [41], and trichome morphology as described by our metric profiles deviated relative to other strains in the experiment. This indicates that the milky phenotype curve is a descriptor of trichome maturation and successful transition from the sessile to capitate-stalked type. Trichome browning was evident in increasing abundance only at the end of the experiment, and thus reflected trichome senescence as shown in previous work [3,10].

6.3. Visual trichome phenotypes are differentiated by trichome fluorescence

6.3.1. Qualitative description of gland fluorescence

The clear, milky and brown phenotypes were distinguished by trichome gland head fluorescence when observed under UV light. Brown trichome heads showed red shifted fluorescence compared to clear and milky trichome heads for all strains in the experiment. The fluorescence within clear, and to a lesser extent milky, trichome gland heads appeared to be localized to cell structures within the gland. Fluorescence intensity formed ring like shapes that appeared to be localized to secretory cells in the trichome gland head, where cannabinoids and cannabinoid precursors such as cannabigerolic acid (CBGA) are produced [31]. Weaker blue fluorescence was also observed in the heads of clear trichomes, increasing in intensity in milky trichomes. The ring like shapes in trichome heads were less defined towards the end of the flowering period, when fluorescence was uniform throughout the trichome head. This was followed by red shift in head fluorescence associated with trichome browning. Weak fluorescence from non-glandular flower tissue was observed in the red channel only, corresponding to chlorophyll content.

6.3.2. Causation of fluorescence in trichomes of cannabis

The reduction in visually localized fluorescence within trichome heads at maturity and senescence suggests reduced accumulation of cannabinoids or the breakdown of existing cannabinoids near secretory cells. When we analysed trichome head fluorescence by raw RGB channel values instead of the CIELAB color space, the green channel intensity increased linearly during flower maturation for all strains, whereas the blue channel plateaued (data not shown) near the harvest window, suggesting accumulation of a blue-green fluorescent substance in the trichome gland head during maturation. Conversely, the blue-green channel fluorescence of non-glandular flower tissue was insignificant over the flowering period, indicating the source of blue-green fluorescence in trichome heads was local secondary metabolites and not inherent to the plant cuticle. Livingston et al. [12] first showed that

fluorescence from the resinous contents in floral trichome heads of hemp shifted from green when sessile to blue when capitate-stalked. Our results confirm these observations and extend the observation period to senescence. Cannabinoids fluoresce blue, even after degradation to CBNA [32], thus red shifted fluorescence upon trichome senescence suggests the accumulation of a non-cannabinoid fluorophore in the gland and cuticle of the trichome head. Trichome head cuticle progressively thickens during trichome maturation, supported by the deposition of cuticle that has migrated through the trichome head embedded in wall matrix with other lipophilic compounds i.e. terpenoids and flavonoids [9,30]. Flavonoids have been detected by green fluorescence in glandular trichomes of multiple plant species [35,36]. Flavonoids are known to protect plant tissues from UV induced damage [37] and are commonly found in the cuticle [38]. In tomato fruit cuticles, flavonoids play a mechanical role by increasing the Young's modulus and elastic phase during fruit ripening [39,40]. Therefore, flavonoids appear to play a role in plant cuticle rigidity, resistance to deformation, and elasticity. When Bergau et al. [36] observed fluorescence in glandular trichomes of a mutant tomato strain, in which flavonoid biosynthesis was suppressed, green autofluorescence of the cuticle was diminished compared to the wild type strain. Taken together, our results in combination with observations from other researchers suggests that trichome head fluorescence in cannabis progresses from green when sessile, to blue fluorescence near the secretory cells and in the trichome gland head due to accumulation of cannabinoids during development [12,32], to blue-green fluorescence due to a non-cannabinoid fluorophore e.g. flavonoids red shifting the fluorescence observed from whole trichome heads during senescence. Further work analyzing the fluorescence emission from maturing and senescent glands using confocal methods, such that cuticle and resin fluorescence are delineated, is necessary to elucidate the causes of trichome gland head fluorescence in more detail.

6.4. Phenotypes and morphology metrics can be manipulated by chemical treatment and stress

6.4.1. Milstop application

When basic potassium bicarbonate (pH 8.0) was applied to cannabis flowers, trichome density and clumping were significantly reduced, reflecting a degradative effect of Milstop on the trichome gland head cuticle. The distance to the nearest trichome was not significantly affected as Milstop applications did not stunt floral bract tissue expansion. Milstop sprays likely induced oxidative stress on the surface of the trichome head cuticle, compromising the gland structure. This was reflected by an increase in the brown phenotype, reduced appearance of the milky phenotype, and the emergence of a red shifted fluorescent mode from Milstop treated trichome heads. Previous work has shown flavonoids to fluoresce green when exposed to a basic solution [33, 34], with fluorescence intensity increasing with the pH of the applied solution. When fluorescence data was analysed by raw RGB values instead of the CIELAB color space (data not shown), Milstop application significantly increased the green channel fluorescence of trichome glands compared to the water treated control, suggesting the presence of a green fluorescent substance that was responsive to pH.

6.4.2. Presumptive viroid disease stress

When cannabis flowers showed signs of stunting due to presumptive virus disease stress, trichome stalk elongation was reduced and trichomes remained sessile, and their diameter as computed by our automatic method was approximately 20 µm smaller than trichomes of healthy flowers, with a mode stunted diameter of approximately 80 µm. Small and Naraine [41] characterized trichome head gland diameter in drug-producing cannabis flowers as well as in hemp (non-psychotropic, non-drug producing) flowers, and showed that the former have larger trichome head diameters at harvest compared to the latter. The average diameter of trichomes heads of hemp in their work was 80 µm, similar to

the predicted trichome head diameter of stunted plants with arrested flower development in this study. Livingston et al. [12] described a developmental and morphological link between sessile and capitate stalked trichomes, reporting that numbers of secretory cells increased together with stalk elongation during the transition from non-stalked sessile trichomes to capitate stalked trichomes. Our results suggest that stunted trichome flower maturation induced by disease stress did not achieve the mature capitate stalked trichome type found on healthy bract tissues. Since trichome stalk elongation is correlated with accumulation of cannabinoids such as THC in the trichome heads, this has important commercial implications. Our automated approach can potentially distinguish trichomes on plants that are subjected to various forms of stress which may influence the accumulation of cannabinoids.

7. Conclusion

The growing environment surrounding cannabis plants can impose various forms of stress, influencing the accumulation of cannabinoids. Cannabis flower development progresses over a 7–8-week period during which glandular trichomes achieve maturation and presumably contain the highest cannabinoid content. Measurements of cannabinoids (THC and CBD in particular) and terpenes are conducted following harvest by commercial testing labs, thus these analyses are not informative during the flowering period. One challenge in the cultivation process is establishing the optimal time to harvest, which can vary according to the cannabis strain and growing conditions. This unpredictability can be reduced by the automated trichome analysis approach we describe here that establishes strain agnostic phenotypes associated with flower development. By combining conventional optics with recent advancements in computer vision, we were able to analyze the details provided in macroscopic photography using the high throughput, data-driven processing capabilities of machine learning, such that the morphological features of developing trichomes could be recorded during cannabis flower maturation for multiple strains *in situ*. The observed relationship between trichome gland head diameter and morphological metrics indicates the feasibility of automatic quality assurance software that can determine how flower maturation is proceeding and if strain specific potential may be attained. Parameterization of flower maturation and trichome development by metrics describing trichome morphology would form a decision space where a classifier or other data driven model could estimate if cannabis flowers are ready for harvest, are subjected to stress or disease, or preferable compared to other candidate strains. The limitations of our work are the fixed bird's eye viewpoint of our observations, limiting detection of occluded trichome glands underneath elongated stalks or resident in folds of bract tissue. The observations made are also limited to a small portion of the bracts on a large inflorescence, although the lack of significant differences in phenotype development at different points within the inflorescence, as outline in Fig. 1, implies that sparse sampling is feasible. Further integration of computer science advances to extract supplementary information describing bract tissue geometry would refine the automatic trichome analysis pipeline. Additionally, we designed a classifier around the clear-milky-brown phenotype as this was the traditional visual description of cannabis glandular trichome maturation, but we have not investigated whether these three classes are optimal for fine grained classification of glandular trichomes. Further work employing purely data driven methods to cluster trichome visual features could be explored to discover additional classes, potentially revealing novel visual descriptors of glandular trichome maturation and flower development in cannabis.

Funding

This work was supported by the Natural Sciences and Engineering Research Council of Canada Alliance grant, jointly with Pure SunFarms, Delta, BC, through a university-industry collaborative project awarded

to Simon Fraser University.

CRediT authorship contribution statement

D.B. Sutton: Conceptualization, Formal analysis, Data curation, Visualization, Writing – original draft, Writing – review & editing. **Z.K. Punja:** Conceptualization, Formal analysis, Writing – original draft, Writing – review & editing, Supervision, Funding acquisition. **G. Hamarneh:** Conceptualization, Formal analysis, Writing – original draft, Writing – review & editing, Supervision, Funding acquisition.

Declaration of Competing Interest

The authors declare that they have no known competing financial interests or personal relationships that could have appeared to influence the work reported in this paper.

Acknowledgements

We thank Alex Cheung, Devin Melnyk, Rob Baldwin, Liam Buirs, and Sam Lung (Pure SunFarms Ltd.) for their assistance with data collection, conducting experiments, and plant propagation.

Supplementary materials

Supplementary material associated with this article can be found, in the online version, at [doi:10.1016/j.atech.2022.100111](https://doi.org/10.1016/j.atech.2022.100111).

References

- [1] T. Seddon, W. Floodgate, W. Cham, *Regulating Cannabis: A global Review and Future Directions*, Springer International Publishing AG, 2020.
- [2] C.M. Andre, J.F. Hausman, G. Guerriero, *Cannabis sativa*: the plant of the thousand and one molecules, *Front. Plant Sci.* 7 (19) (2016), <https://doi.org/10.3389/fpls.2016.00019>.
- [3] David JP Potter, *The propagation, Characterisation and Optimisation of Cannabis sativa L. As a Phytopharmaceutical*, Kings College, University of London, 2009. PhD thesis.
- [4] J. Meija, G. McRae, C.O. Miles, J.E. Melanson, Thermal stability of cannabinoids in dried cannabis: a kinetic study, *Anal. Bioanal. Chem.* 414 (2022) 349–359.
- [5] B. Dell, A.J. McComb, Plant resins – their formation, secretion and possible functions, *Adv. Bot. Res.* 6 (1979) 277–316, [https://doi.org/10.1016/S0065-2296\(08\)60332-8](https://doi.org/10.1016/S0065-2296(08)60332-8).
- [6] D.A. Levin, The role of trichomes in plant defense, *Q. Rev. Biol.* 48 (1) (1973) 3–15.
- [7] C.T. Hammond, P.G. Mahlberg, Morphology of glandular hairs of *Cannabis sativa* from scanning electron microscopy, *Am. J. Bot.* 60 (6) (1973) 524–528, <https://doi.org/10.2307/2441375>.
- [8] C.T. Hammond, P.G. Mahlberg, Morphogenesis of capitate glandular hairs of *Cannabis sativa*, *Am. J. Bot.* 64 (8) (1977) 1023–1031, <https://doi.org/10.2307/2442258>.
- [9] P.G. Mahlberg, E.-S. Kim, Cuticle development on glandular trichomes of *Cannabis sativa* (Cannabaceae), *Am. J. Bot.* 78 (8) (1991) 1113–1122, <https://doi.org/10.1002/j.1537-2197.1991.tb14518.x>.
- [10] P.G. Mahlberg, E.S. Kim, Accumulation of cannabinoids in glandular trichomes of cannabis (Cannabaceae), *J. Ind. Hemp* 9 (1) (2004) 15–36, https://doi.org/10.1300/J237v09n01_04.
- [11] S. Sirikantaramas, F. Taura, Y. Tanaka, Y. Ishikawa, S. Morimoto, Y. Shoyama, Tetrahydrocannabinolic acid synthase, the enzyme controlling marijuana psychoactivity, is secreted into the storage cavity of the glandular trichomes, *Plant Cell Physiol.* 46 (9) (2005) 1578–1582, <https://doi.org/10.1093/pcp/pci166>.
- [12] S.J. Livingston, T.D. Quilichini, J.K. Booth, D.C.J. Wong, K.H. Rensing, J. Laflamme-Yonkman, S.D. Castellarin, J. Bohlmann, J.E. Page, A.L. Samuels, Cannabis glandular trichomes alter morphology and metabolite content during flower maturation, *Plant J.* 101 (2019) 37–56, <https://doi.org/10.1111/tpj.14516>.
- [13] C.A.S. Tanney, R. Backer, A. Geitmann, D.L. Smith, Cannabis glandular trichomes: a cellular metabolite factor, *Front. Plant Sci.* (2021) 12, <https://doi.org/10.3389/fpls.2021.721986>.
- [14] J.C. Turner, J.K. Hemphill, P.G. Mahlberg, Gland distribution and cannabinoid content in clones of *Cannabis sativa* L, *Am. J. Bot.* 64 (6) (1977) 687–693, <https://doi.org/10.2307/2441721>.
- [15] N. Bergau, A.N. Santos, A. Henning, G.U. Balcke, A. Tissier, Autofluorescence as a signal to sort developing glandular trichomes by flow cytometry, *Front. Plant Sci.* 7 (2016), <https://doi.org/10.3389/fpls.2016.00949>.
- [16] H. Failmezger, B. Jaegle, A. Schrader, M. Hulskamp, A. Tresch, Semi-automated 3D leaf reconstruction and analysis of trichome patterning from light microscopic images, *PLoS Comput. Biol.* 9 (4) (2013), <https://doi.org/10.1371/journal.pcbi.1003029>.

- [17] S.V. Mirnezami, T. Young, T. Assefa, S. Prichard, K. Nagasubramanian, S. Sarkar, S. Sundararajan, M.E. O’Neal, B. Ganapathysubramanian, A. Singh, Automated trichome counting in soybean using advanced image-processing techniques, *Appl. Plant Sci.* 8 (7) (2020) doi:10.1002/2Faps.3.11375.
- [18] V. Rolland, M.R. Farazi, W.C. Conaty, D. Cameron, S. Liu, L. Petersson, W.N. Stiller, Hairnet: a deep learning model to score leaf hairiness, a key phenotype for cotton yield, value and insect resistance, *Plant Methods* 18 (8) (2022), <https://doi.org/10.1186/s13007-021-00820-8>.
- [19] T. Overton, A. Tucker, DO-U-Net for segmentation and counting, in: M.R. Berthold, A. Feelders, G. Kreml (Eds.), *Advances in Intelligent Data Analysis XVIII*, Springer International Publishing, 2020, pp. 391–403, https://doi.org/10.1007/978-3-030-44584-3_31.
- [20] I.F. Sbalzarini, Seeing is believing: quantifying is convincing: computational image analysis in biology. *Focus on Bio-Image Informatics*, 2016, pp. 1–39, https://doi.org/10.1007/978-3-319-28549-8_1.
- [21] F. Cascini, C. Aiello, G. Di Tanna, Increasing delta-9-tetrahydrocannabinol (-9-thc) content in herbal cannabis over time: systematic review and meta-analysis, *Curr. Drug Abuse Rev.* 5 (1) (2012) 32–40, <https://doi.org/10.2174/1874473711205010032>.
- [22] J.K. Booth, J.E. Page, J. Bohlmann, Terpene synthases from *Cannabis sativa*, *PLoS ONE* 12 (3) (2017), <https://doi.org/10.1371/journal.pone.0173911>.
- [23] L.J. Conneely, R. Mauleon, J. Mieog, B.J. Barkla, T. Kretzschmar, Characterization of the *Cannabis sativa* glandular trichome proteome, *PLoS ONE* 16 (4) (2021), <https://doi.org/10.1371/journal.pone.0242633>.
- [24] Z.K. Punja, J.E. Holmes, Hermaphroditism in marijuana (*Cannabis sativa* L.) inflorescences – impact on floral morphology, seed formation, progeny sex ratios, and genetic variation, *Front. Plant Sci.* 11 (2020), <https://doi.org/10.3389/fpls.2020.00718>.
- [25] C. Meier, V. Mediavilla, Factors influencing the yield and quality of hemp (*Cannabis sativa* L.) essential oil, *J. Int. Hemp Assoc.* 5 (1998) 16–20.
- [26] E. Naim-Feil, E.J. Breen, L.W. Pembleton, L.E. Spooner, G.C. Spangenberg, N.O. I. Cogan, Empirical evaluation of inflorescences’ morphological attributes for yield optimization of medicinal cannabis cultivars, *Front. Plant Sci.* (2022) 13, <https://doi.org/10.3389/fpls.2022.858519>.
- [27] J.C. Turner, J.K. Hemphill, P.G. Mahlberg, Interrelationships of glandular trichomes and cannabinoid content. I. Developing pistillate bracts of *Cannabis sativa* L. (Cannabaceae), *Bull. Narc.* 33 (2) (1981) 59–69.
- [28] E.-S. Kim, P.G. Mahlberg, Immunochemical localization of tetrahydrocannabinol (THC) in cryofixed glandular trichomes of cannabis (cannabaceae), *Am. J. Bot.* 84 (3) (1997) 336–342.
- [29] P.G. Mahlberg, E.S. Kim, Secretory vesicle formation in glandular trichomes of *Cannabis sativa* (Cannabaceae), *Am. J. Bot.* 79 (2) (1992) 166–173, <https://doi.org/10.2307/2445104>.
- [30] S.J. Livingston, E.J. Bae, F. Unda, M.G. Hahn, S.D. Mansfield, J.E. Page, A. L. Samuels, Cannabis glandular trichome cell walls undergo remodeling to store specialized metabolites, *Plant Cell Physiol.* 62 (12) (2021) 1944–1962, <https://doi.org/10.1093/pcp/pcab127>.
- [31] P. Ebersbach, F. Stehle, O. Kayser, E. Freier, Chemical fingerprinting of single glandular trichomes of *cannabis sativa* by coherent anti-Stokes Raman scattering (CARS) microscopy, *BMC Plant Biol.* 18 (275) (2018), <https://doi.org/10.1186/s12870-018-1481-4>.
- [32] A. Hazekamp, A. Peltenburg, R. Verpoorte, C. Giroud, Chromatographic and spectroscopic data of cannabinoids from *Cannabis sativa* L., *J. Liquid Chromatogr. Related Technol.* 28 (15) (2005) 2361–2382, <https://doi.org/10.1080/10826070500187558>.
- [33] T.H. Lam, S. Chen, Y.B. Ho, Observations on ultraviolet-fluorescent trichomes on the tepals of narcissus flowers, *Plant Sci. Lett.* 18 (1980) 115–120.
- [34] O. Monago-Marana, I. Duran-Meras, T. Galeano-Diaz, A. Munoz de la Pena, Fluorescence properties of flavonoid compounds: quantification in paprika samples using spectrofluorimetry coupled to second order chemometric tools, *Food Chem.* 196 (2016) 1058–1065, <https://doi.org/10.1016/j.foodchem.2015.10.041>.
- [35] V.V. Roshchina, A.V. Kuchin, V.A. Yashin, Application of autofluorescence for analysis of medicinal plants, *Int. J. Spectrosc.* (2017), <https://doi.org/10.1155/2017/7159609>.
- [36] N. Bergau, S. Bennewitz, F. Syrowatka, G. Hause, A. Tissier, The development of type VI glandular trichomes in the cultivated tomato *Solanum lycopersicum* and a related wild species *S. habrochaites*, *BMC Plant Biol.* 15 (289) (2015), <https://doi.org/10.1186/s12870-015-0678-z>.
- [37] M. Sisa, S.L. Bonnet, D. Ferreira, J.H. Van der Westhuizen, Photochemistry of flavonoids, *Molecules* 15 (8) (2010) 5196–5245, <https://doi.org/10.3390/molecules15085196>.
- [38] N. Reynoud, J. Petit, C. Bres, M. Lahaye, C. Rothan, D. Marion, B. Bakan, The complex architecture of plant cuticles and its relation to multiple biological functions, *Front. Plant Sci.* 12 (2021), <https://doi.org/10.3389/fpls.2021.782773>.
- [39] L. Espana, J.A. Heredia-Guerrero, J.J. Reina-Pinto, R. Fernandez-Munoz, A. Heredia, E. Dominguez, Transient silencing of chalcone synthase during fruit ripening modifies tomato epidermal cells and cuticle properties, *Plant Physiol.* 166 (3) (2014) 1371–1386, <https://doi.org/10.1104/pp.114.246405>.
- [40] H. Bargel, C. Neinhuis, Altered tomato fruit cuticle biomechanics of a pleiotropic non ripening mutant, *J. Plant Growth Regul.* 23 (2004) 61–75, <https://doi.org/10.1007/s00344-004-0036-0>.
- [41] E. Small, S.G.U. Naraine, Size matters: evolution of large drug-secreting resin glands in elite pharmaceutical strains of *cannabis sativa* (marijuana), *Genet. Resour. Crop Evol.* 63 (2) (2015) 349–359, <https://doi.org/10.1007/s10722-015-0254-2>.